INELASTIC DISPLACEMENT PATTERNS IN SUPPORT OF DIRECT DISPLACEMENT-BASED DESIGN FOR CONTINUOUS BRIDGE STRUCTURES

Hazim M. Dwairi and Mervyn J. Kowalsky

Department of Civil, Construction and Environmental Engineering, North Carolina State University, Campus-Box 7908, Raleigh, NC-27695, USA

SUMMARY

Target-displacement profiles have a significant impact on the end result of direct displacement-based design (DDBD). Therefore establishing a realistic and achievable target profile is a necessity for the design procedure. In this study inelastic time history analyses were conducted for six multi-span bridge configurations. Parameters considered included bridge geometry, superstructure and substructure stiffness, abutment type, and earthquake record. Three inelastic displacement pattern scenarios were identified: (1) rigid body translation (2) rigid body translation with rotation and, (3) flexible pattern. These displacement patterns were identified based on the relative stiffness between the superstructure and substructure. The first and second scenarios require minimal effort in the design, since no iterations are needed to define the target-displacement profile. However, an iterative algorithm is presented to design for the third scenario. A series of bridges with various configurations was designed using DDBD for rigid body translation and flexible superstructure scenarios. The designs for the flexible scenario showed good agreement with selected target profiles for bridges with up to 5 spans. However, significant errors in selecting target profiles were noted for some bridges with a larger number of spans.

KEY WORDS

Inelastic Displacement Patterns; Direct Displacement-based Design; Continuous Bridges.

1. INTRODUCTION

With the advent of performance-based earthquake engineering, the need for a comprehensive, yet simple, design approach is significant. Such approaches should allow the engineer to control the bridge displacement profile, and hence damage, for a variety of performance limit states and earthquake intensities. One such approach is direct displacement-based design (DDBD). In the DDBD method, a structure is designed such that a predefined displacement limit is achieved when the structure is subjected to a predefined earthquake that is consistent with that assumed for the design. The DDBD procedure, when applied to single column bridges was shown to provide excellent control over displacements and hence damage, across a wide range of column configurations [1]. This was evaluated by comparing the maximum displacements from dynamic inelastic time history analyses conducted on columns designed with DDBD to the target displacements specified during the designs. The DDBD procedure for single-degree-of freedom (SDOF) structures starts with selecting a target displacement that corresponds to the desired level of damage. An equivalent linear SDOF structure is then characterized by the secant stiffness to maximum response and equivalent viscous damping. The required effective period of the equivalent structure is then determined using the elastic design spectra reduced based upon the equivalent damping value.

Given the expectation that damage will occur in moderate to large earthquakes, it is logical that the design methodology employed should (1) directly address the issue of inelastic behavior, and (2) Provide a method for controlling the amount of damage which occurs. However, current design approaches, which are predominantly force-based in nature, cannot reliably meet these needs largely because forces are poor indicators of damage potential. In order to specify damage for a given seismic event, it is necessary to specify deformation. While agreement may not be uniform, deformation quantities such as material strains are much more reliable indicators of performance than forces. Furthermore, strains can be correlated to inelastic displacements, which can then be used in the DDBD approach. However, before inelastic displacement can be specified, the mechanisms by which a complex structure deforms inelastically must first be understood. As a result, the primary

objective of this paper is to develop the tools – specifically, methods for establishing inelastic displacement patterns for multi-span bridges, that can then be applied in a direct displacement-based seismic design approach.

The first effort at extending the DDBD approach initially proposed by Priestley [2] to multi-span bridges was carried out by Calvi and Kingsley in 1995 [3]. In order to extend the procedure to multiple degree of freedom systems (MDOF), it is necessary to first characterize an equivalent single-degree-of freedom system with the following parameters: system displacement, system damping, and system mass. The equivalent system displacement was proposed as the displacement that resulted in work equivalence between the equivalent SDOF system and the MDOF system. The equivalent damping was obtained using the *substitute structure* procedure proposed by Shibata and Sozen in 1976 [4], which weighs the effective system damping of each element in proportion to the flexural strain energy of each element. The equivalent system mass was defined based on force equivalence between the SDOF and MDOF systems. Applying these definitions to the design approach resulted in reasonable results for simple symmetric systems, however, for more complex systems, gross errors between expected and actual displacements occurred.

Kowalsky [5] [6], proposed a similar definition for an equivalent SDOF system for multi-span bridges. The primary difference in characterizing the equivalent SDOF system was in the definition of the system damping, whereby the individual member damping values were weighted in proportion to the work done by each member. As a result, members such as abutments, which dissipate energy through the soil, could be modeled along with the column members. A more significant aspect of the research was related to the characterization of the target displacement profile. It was proposed that the displacement profile should be obtained by performing a modal analysis using reduced stiffness properties to account for the expected level of inelastic deformation. Kowalsky [6] proposed the *effective mode shape* method that utilizes column secant stiffnesses in the modal analysis process to establish 'effective mode shapes'. These mode shapes are then used to determine a displacement pattern via modal combination. In order to obtain the target-displacement profile, the displacement pattern is then scaled such that at least one column reaches its intended damage level based on the strain criteria. The approach is iterative in nature and is embedded within the displacement-

based design procedure. As a result, it can be time consuming although simplified by the use of computers. Furthermore, in some cases, such a complex approach may not be needed.

The research in this paper aims to: (1) Identify the classes of displacement patterns typically encountered in bridge design, (2) Identify when such patterns are likely to occur, and (3) Apply the results to DDBD while demonstrating its application and providing a suite of analysis results for verification.

2. EVALUATION OF INELASTIC DISPLACEMENT PATTERNS

In order to obtain the target-displacement profile, two parameters need to be specified: (1) amplitude and, (2) displacement pattern. The amplitude depends on the displacement of the critical column, which is defined as the first member to reach its limit state based on a presumed displacement pattern. As mentioned earlier, limit states are usually expressed in terms of strain levels consistent with the desired levels of damage. Once these strain levels are selected, corresponding "damage displacements" are estimated [7] resulting in a damage envelope that controls the amplitude of the target-displacement profile. The relationships between the damage and its corresponding limit state are beyond the scope of this paper.

Inelastic displacement patterns depend on the bridge geometry, superstructure and substructure stiffness and abutment type. Consider the inelastic pattern scenarios shown in Figure 1; scenarios 'a' and 'b' represent a rigid body translation where all members translate the same amount. Such a scenario is expected to occur in the case of a rigid superstructure with no eccentricity between center of mass and center of rigidity. Scenarios 'c' and 'd' represent a rigid body translation with rotation, which is expected to occur in the case of a rigid superstructure with eccentricity between the center of mass and the center of rigidity. The third scenario is the one shown as 'e' and 'f', which represents a flexible pattern. This scenario may correspond to the first mode or higher modes of the structure depending on the geometry and regularity of the bridge.

2.1 Study Parameters and Analysis Algorithm

In order to identify the inelastic displacement patterns of continuous bridges, a series of four

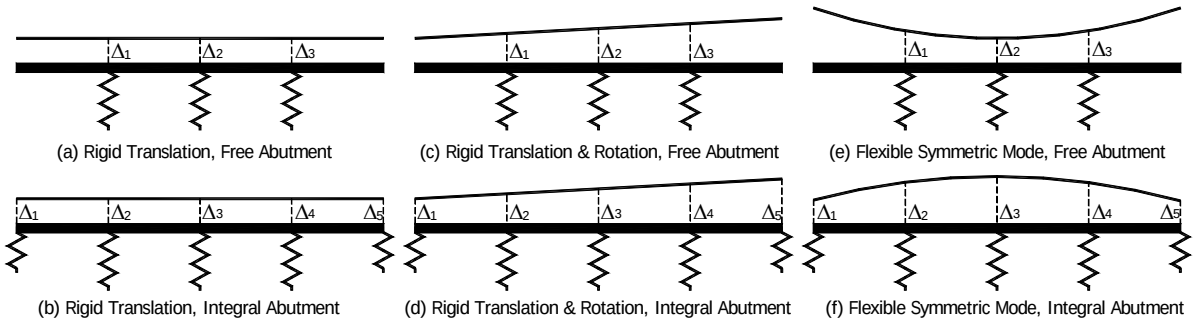

Figure 1 Inelastic Displacement Pattern Scenarios for Continuous Bridge Structures, Plan View

span bridge structures subjected to 12 earthquake records was analyzed using inelastic time history analysis. The earthquake records were scaled to 1.0g PGA. The bridges considered range from regular symmetric to irregular asymmetric as shown in Figure 2. Each of the bridges was assumed to be with and without abutment restraint in the transverse direction. In the case of a restrained abutment, it was assumed that the superstructure is integrally built into the abutment which provides the superstructure with translational stiffness and no rotational restraint. Abutment stiffness was estimated for yield displacements of 25mm and 60mm, based on CALTRANS memo 5-1 [8]. In the structural model used in the analyses, the abutments were modeled as translational springs that follow a bilinear with slackness hysteresis as shown in Figure 3; a gap of 40mm and a bilinear factor (r) of 5% were used.

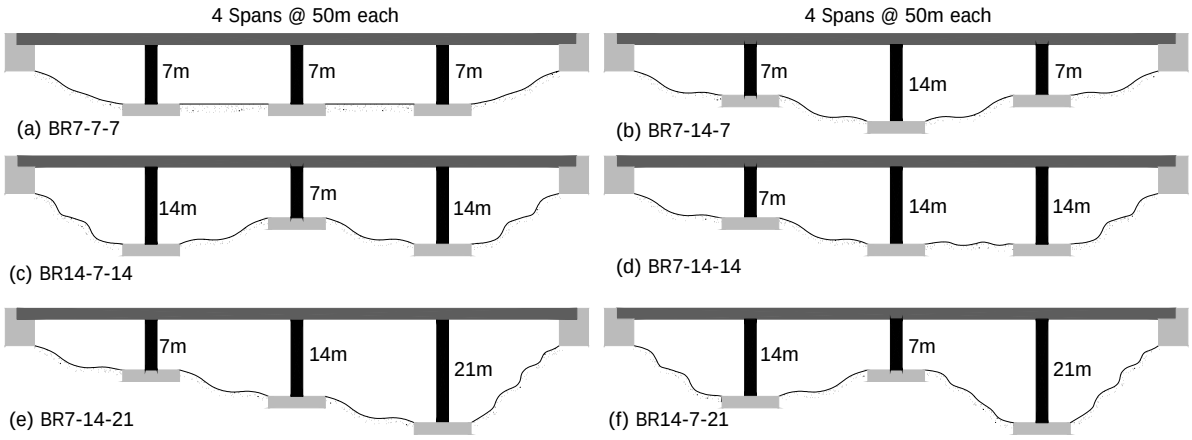

Figure 2 Muli-Span Bridge Configurations Considered in the Study.

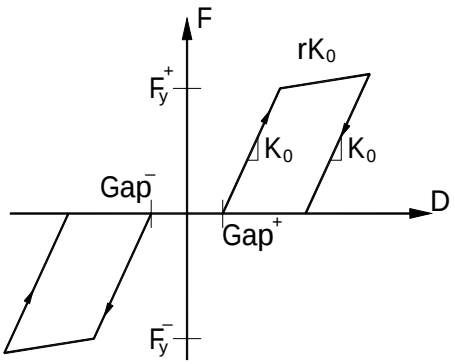

Figure 3 Bilinear with Slackness Hysteretic Model, [9].

The inelastic displacement patterns are believed to be highly dependent on the superstructure to substructure stiffness ratio; hence the superstructure moment of inertia around the vertical axis was varied between $5m^4$ and $500m^4$, although the majority of bridges in practice have moment of inertia values between $50m^4$ and $150m^4$. The pier yield strengths were varied between 2,000KN.m and 24,000KN.m. All columns were assumed to have a diameter of 1.5m and equal reinforcement ratio; as a result all columns have equal yield curvature and base moment. The modified Takeda hysteretic model [10] was used to describe the column inelastic behavior. Inelastic time history analyses were carried out for all the bridges using RUAUMOKO [9], a dynamic analysis software package. Table 1 summarizes all the study parameters. The total number of bridge structures analyzed in this study was about 16,500.

Table 1 Summary of Study Parameters.

Bridge Configuration	Abutment Type	Pier Yield Moment (KN.m)	Superstructure Moment of Inertia (m^4)	Earthquake Record
BR7-7-7	Free	2,000	5	Taft
BR7-14-7	Integral (D_y=25mm)	4,000	10	Pacoima
BR14-7-14	Integral (D_y=60mm)	8,000	25	El Centro
BR7-14-14		12,000	50	Duze
BR7-14-21		16,000	75	Kobe
BR14-7-21		20,000	100	Northridge
		24,000	125	Tabas
			150	Santa Barbara
			200	Nahanni
			350	Big Bear
			500	Gazli
				El Alamo

In order to classify these bridges, the relative stiffness ratio (RS) between the superstructure and substructure was used. The deck was modeled as a beam pinned from both ends, and its stiffness (Ks) was calculated as the force which will cause a unit displacement at mid-span, as shown in Figure 4a. It is well accepted to assume that the deck will remain elastic under the design earthquake; therefore, the gross moment of inertia was utilized for superstructure stiffness calculations. On the other hand, the piers were modeled as double bending cantilevers, and their cracked stiffnesses (Kc) were calculated for a unit displacement at the free end, as shown in Figure 4b. The resulting relative stiffness (RS) is given by Eq. 1.

$$RS = \frac{Ks}{n}\sum_{i=1}^{n}\frac{1}{Kc_i} = \frac{8}{n}\sum_{i=1}^{n}\frac{Is \times hc_i^3}{Ic_i \times Ls^3} \qquad \textbf{Eq. 1}$$

In Eq. 1 *n* is number of piers, *Ic* is pier cracked section moment of inertia, *hc* is the pier height, *Is* is the deck gross moment of inertia and *Ls* is the deck total length.

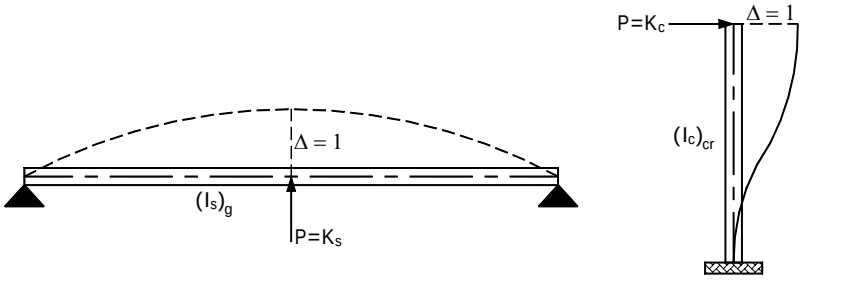

(a) Deck Modeling for RS Calculation, (Plan View)

(b) Pier Modeling for RS Calculation, (Elevation)

Figure 4 Relative Stiffness (RS) Calculation.

For each of the cases the displacement envelopes were determined, which in most instances were close to the actual displacement profile. In the case where the superstructure can be assumed to be rigid, all the points on the deck are expected to translate the same amount, which results in a theoretical coefficient of variation for the deck displacements equal to 0. However, in the event that the superstructure is rigid with an eccentricity between the center of mass and the center of rigidity all the points on the deck are expected to have equal rotations, which also results in a 0 coefficient of variation for the deck rotations. In the case of a flexible superstructure, the deck is expected to have a flexible displacement pattern

with a coefficient of variation greater than 0. It is suggested that if the displacement pattern has a coefficient of variation greater than 10%, it should be considered flexible. The following section presents and discusses the analyses results.

2.2 *Rigid Body Translation Displacement Pattern (RBT)*

Only symmetric bridges are expected to have a RBT pattern, thus the coefficient of variation of displacements envelope was plotted against the relative stiffness as shown in Figure 5 through Figure 7. As the relative stiffness increases, either the superstructure stiffness increases or the substructure stiffness decreases. Note that there is more than one combination of superstructure and substructure stiffnesses that results in the same relative stiffness. Each symbol on these figures represents one of the earthquakes given in Table 1.

Shown in Figure 5 through Figure 7 are the results for three symmetric bridges. Recall that a bridge with a RBT scenario is defined as having a coefficient of variation of the displacement profile, equal to or less than 10%. A RBT scenario was identified for all three bridges with free abutments, while no apparent trend was identified for bridges with integrally built abutments. Based on the results presented in Figure 5, a bridge with free abutments and all piers having the same height could have a RBT scenario if its relative stiffness is equal to or greater than 1. In addition, a bridge with the middle pier twice the height of the side piers is expected to have a RBT scenario if its relative stiffness is equal to or greater than 2, see Figure 6. However, a bridge with the middle pier half the height of the side piers is expected to have a RBT scenario if its relative stiffness is equal to or greater than 3, see Figure 7. Theoretically, bridges with integrally built abutments could have a rigid body translation pattern in the case of an extremely rigid superstructure, however, based on the results from the previous figures this could only happen for structures with impractical relative stiffnesses. At low relative stiffness values (i.e a flexible superstructure or weak piers), bridges with free abutments had higher coefficient of variations than bridges with integrally built abutments, which could be attributed to the excessive movement of the superstructure at the free ends. It is noted that the stiffness of integrally built abutments, chosen based on the CALTRANS memo 5-1, did not have any significant effect on the

inelastic displacement pattern. Also the vast majority of bridges with integral abutments are expected to have a flexible scenario with coefficients of variation less than 50%.

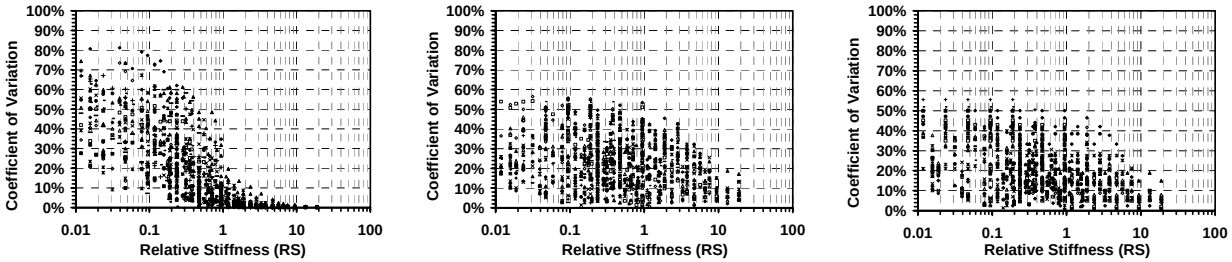

(a) Free Abutment (b) Integral Abutment, Δ_y= 25mm (c)Integral Abutment, Δ_y= 60mm

Figure 5 Coefficients of Variation for the Displacement Envelopes of BR7-7-7

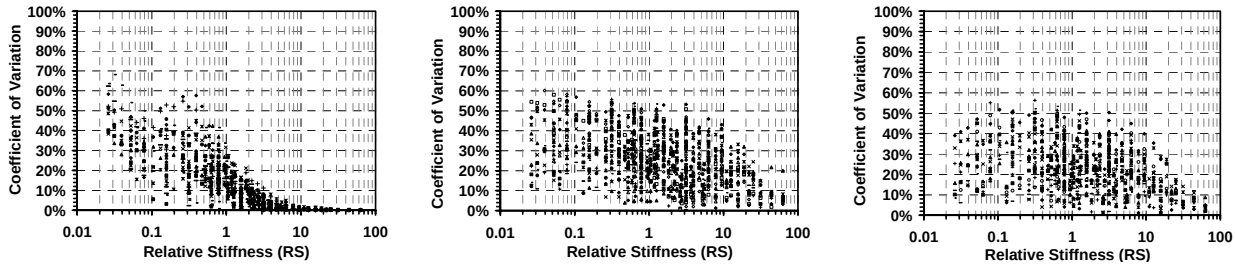

(a) Free Abutment (b) Integral Abutment, Δ_y= 25mm (c) Integral Abutment, Δ_y= 60mm

Figure 6 Coefficients of Variation for Displacement Envelopes of BR7-14-7

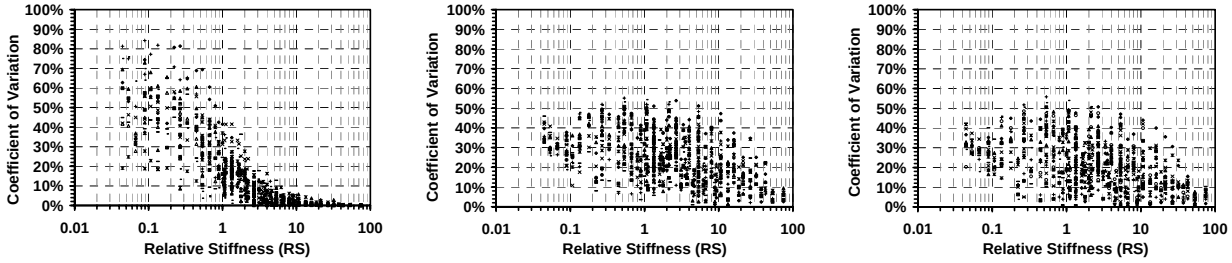

(a) Free Abutment (b) Integral Abutment, Δ_y= 25mm (c) Integral Abutment, Δ_y= 60mm

Figure 7 Coefficients of Variation for Displacement Envelopes of BR14-7-14

2.3 Rigid Body Translation with Rotation Displacement Pattern (RBTR)

Shown in Figure 8 through Figure 10 are the results for three asymmetric bridge structures. Such bridges with rigid superstructures are expected to exhibit a rigid body translation and rotation due to their asymmetric geometry. The coefficients of variation shown are for the rotations of all the nodes used to model the deck behavior. Similar to the symmetric bridges, it was possible to identify a rigid body translation with rotation displacement pattern only for

free abutment bridges, while no such pattern was identified for bridges with integrally built abutments. Based on the results presented, a bridge with one side pier half the height of the other two is expected to have a RBTR scenario if its relative stiffness is greater than 6. However, a bridge of the form L-2L-3L with relative stiffness greater than or equal to 10 is expected to have a RBTR displacement pattern. On the other hand, a highly irregular asymmetric bridge of the form 2L-L-3L is expected to have a RBTR scenario if its relative stiffness is greater than or equal to 12. In Figure 8 through Figure 10, it is apparent that the stiffness of the integrally built abutment has no significant effect on the displacement pattern. The vast majority of bridges with integral abutments are expected to have a flexible scenario with coefficients of variation of deck rotations less than 50%.

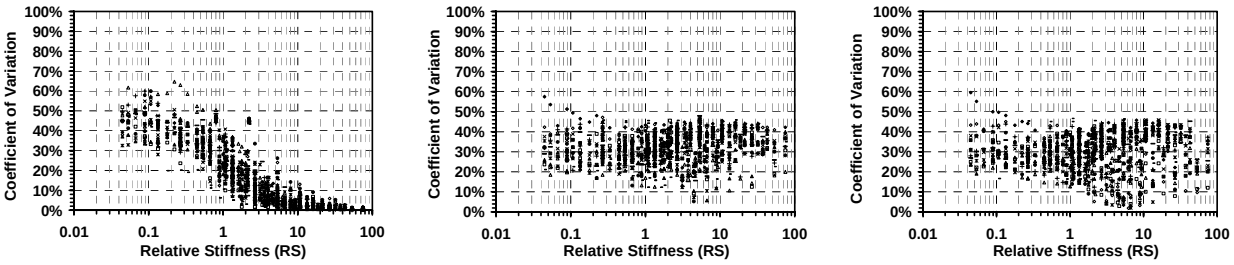

(a) Free Abutment (b) Integral Abutment, Δ_y= 25mm (c) Integral Abutment, Δ_y= 60mm

Figure 8 Coefficients of Variation for Rotation Envelopes of BR7-14-14

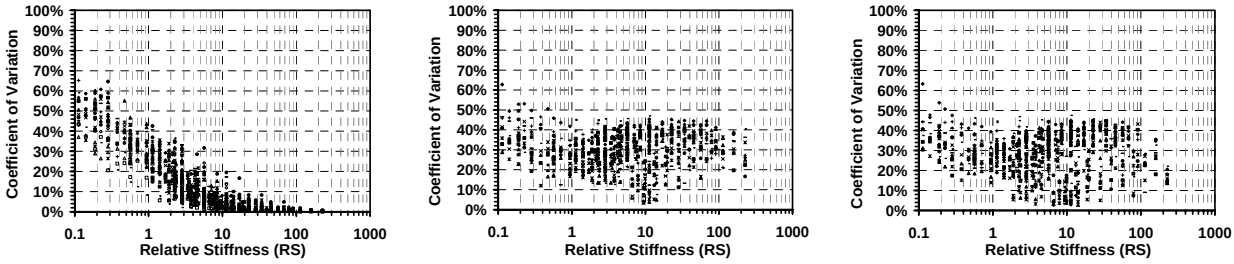

(d) Free Abutment (e) Integral Abutment, Δ_y= 25mm (f) Integral Abutment, Δ_y= 60mm

Figure 9 Coefficients of Variation for Rotation Envelopes of BR7-14-21

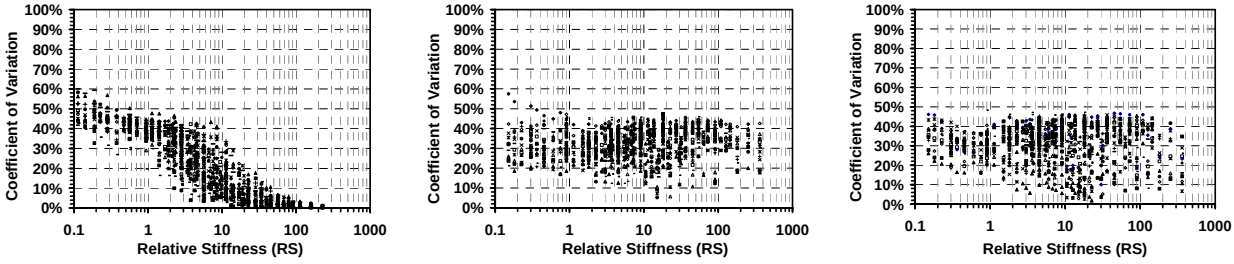

(g) Free Abutment (h) Integral Abutment, Δ_y= 25mm (i) Integral Abutment, Δ_y= 60mm

Figure 10 Coefficients of Variation for Rotation Envelopes of BR14-7-21

2.4 *Flexible Displacement Pattern*

It is evident based on the previous discussion that the vast majority of bridge structures will deform in a flexible mode like the ones shown in Figure 1e and Figure 1f. The flexible displacement pattern could be either symmetric or asymmetric based on the bridge geometry and stiffness distribution across the bridge. In the case of a flexible superstructure, columns are not expected to deform independent of each other like the theoretical case of an infinitely flexible superstructure, or deform in the same amount as the rigid body translation case. Instead, the displacement pattern is expected to be a function of the bridge mode shapes, which in turn are a function of the relative superstructure to substructure stiffness.

These mode shapes, which should be used to obtain the displacement pattern, are also a function of the design limit state. In the case of structures that will be designed for essentially elastic limit states, such as the serviceability limit state, it is apparent that the mode shapes used to obtain the target profile should be based on elastic properties of the structure. However, in the case where structures are designed to the damage-control limit states, where members are expected to respond inelastically, it is necessary to consider effective properties (secant stiffness to maximum response) of the structure in the mode shape calculations. Kowalsky [6] proposed the *effective mode shape* (EMS) method to obtain target-displacement profile for inelastic systems. The method is iterative in nature and embedded in the displacement-based design procedure, and it comprises the following steps:

1. **Evaluate Mode Shapes (ϕ_j):** When identifying a displacement pattern, structure properties are not available, thus a first estimate is required to start the procedure. It is well accepted to assume that the superstructure will respond elastically, therefore its elastic properties should be used. However, it is suggested that a stiffness equal to 10% of the uncracked section stiffness be applied to columns expected to deform inelastically. While a stiffness equal to 60% of the uncracked section stiffness is proposed to be used for columns that are expected to remain elastic. If the abutments are assumed to deform elastically then 30% of their initial elastic stiffness should be used. Once the structure properties have been established, any computer program or

hand calculations could be used to solve the eigenvalue problem and obtain the mode shapes.

2. **Evaluate Modal Participation Factors (P_j):** The modal participation factors can be computed as given in Eq. 2.

$$P_j = \frac{\phi_j M r}{\phi_j^T M \phi_j} \qquad \textbf{Eq. 2}$$

Where M represents a diagonal mass matrix and r is a unit vector.

3. **Evaluate Bent Modal Displacements:** Compute the expected modal displacement of each bent according to Eq. 3 where index i represents the bent number, index j represents the mode number, $\phi_{i,j}$ is the modal factor of bent i and mode j, and Sd_j is the spectral displacement for mode j obtained by entering the 5% damped design spectra with the modal period obtained from the modal analysis.

$$\Delta_{i,j} = \phi_{i,j} P_j Sd_i \qquad \textbf{Eq. 3}$$

4. **Evaluate Expected Displacement Pattern:** Finally, the displacement pattern is obtained by any appropriate combination of the modal displacements. Such a combination can be computed as square root of the sum of squares (SRSS) as given by Eq. 4. However, complete quadratic combination (CQC) is expected to yield better results when the natural frequencies of the participating modes in the response are not well-separated.

$$\Delta_i = \sqrt{\sum_j \Delta_{i,j}^2} \qquad \textbf{Eq. 4}$$

In order to obtain target-displacement profile, the displacement pattern given by Eq. 4 is then scaled such that none of the column displacements exceed the target displacements obtained based upon strain criteria.

Once the target-displacement profile has been established, the displacement-based design steps described in section 3 are followed. As a result, the member design forces are known and can be used to compute member secant stiffnesses as given by Eq. 5 where V_i is the member design shear force. If the revised secant stiffnesses differ significantly from the

assumed values, then the revised stiffness values are used in the modal analysis to obtain a revised target-displacement profile, and the entire design procedure is repeated again until convergence is achieved.

$$K_{eff_i} = V_i / \Delta_i \qquad \textbf{Eq. 5}$$

3. DDBD PROCEDURE FOR MULTI-SPAN BRIDGE STRUCTURES

As mentioned earlier, DDBD aims to design a structure to achieve a prescribed limit state that may be defined directly from displacements or derived from strain criteria under a prescribed earthquake intensity. The procedure utilizes the elastic response spectra reduced for an equivalent damping value and the secant stiffness at peak response. The procedure characterizes the MDOF structure as an equivalent SDOF based on the *substitute structure* concept [4]. The equivalent SDOF inelastic response is represented by the secant stiffness at peak response and equivalent damping value based on Jacobsen's approach [11]. A flowchart of the DDBD procedure is shown in Figure 13 and Figure 14. Note that the flowchart has been divided into two figures for clarity. The user must always start with Figure 13, and may or may not need the portion of the flowchart shown in Figure 14, depending on the characteristics of the displacement pattern. The DDBD procedure for a MDOF bridge is discussed in detail in the following steps:

1. **Select a Displacement Pattern**: As a starting point, assume the cracked section stiffness of all columns is equal to 60% of the uncracked section stiffness. Assume also the seismic force carried by the abutments is equal to 30% of the total seismic force carried by the bridge. Compute the relative stiffness (RS) and determine whether the bridge has a rigid or flexible displacement pattern based upon the results from section 2.
2. **Define Target-Displacement Profile**: In the case of a rigid displacement pattern, the target-displacement profile is obtained by scaling the selected pattern to match the critical column limit-state displacement. In the case of a flexible pattern, follow the *effective mode shape* method discussed in the previous section.

3. **Define an Equivalent SDOF Structure**: Based on research conducted by Calvi and Kingsley [3], an equivalent SDOF structure is established based on equal work done by the MDOF bridge and the equivalent SDOF structure. The equivalent SDOF structure is described by a system displacement and a system mass as given by Eq. 6 and Eq. 7, respectively.

$$\Delta_{sys} = \frac{\sum m_i \Delta_i^2}{\sum m_i \Delta_i} \qquad \textbf{Eq. 6}$$

$$M_{sys} = \frac{1}{\Delta_{sys}} \sum m_i \Delta_i \qquad \textbf{Eq. 7}$$

In Eq. 6 and Eq. 7, m_i is the inertia mass associated with bent 'i' and Δ_i is the target-displacement of bent 'i'.

4. **Estimate Level of Equivalent Viscous Damping**: Utilizing the chosen target displacement for each column and estimated yield displacements, the ductility level is calculated for each member. Yield displacements are estimated using Eq. 8 and Eq. 9 where ε_y is the reinforcement yield strain, D is the circular section diameter and h_c is the rectangular section depth [12].

Circular Concrete Column: $\phi_y = 2.25\varepsilon_y / D$ **Eq. 8**

Rectangular Concrete Column: $\phi_y = 2.10\varepsilon_y / h_c$ **Eq. 9**

Utilizing Jacobsen's approach [11] and assuming an appropriate hysteretic model, a relationship between hysteretic damping and ductility is obtained. Such a relationship, which was obtained by Dwairi *et al.* [13], is shown in Figure 11 and given by Eq. 10 and Eq. 11 for Takeda's hysteretic model [10]. For instance, a R/C column with displacement ductility of 2 is expected to have 8% hysteretic damping. Additional 0%-5% elastic viscous damping (ξ_v) should be added to obtain the level of equivalent viscous damping in accordance with the approach proposed by Grant *et al.* [14].

R/C Column: $\xi_i = \xi_v + \frac{50}{\pi}\left(\frac{\mu - 1}{\mu}\right)\%$ **Eq. 10**

R/C Beam: $\xi_i = \xi_v + \frac{65}{\pi}\left(\frac{\mu - 1}{\mu}\right)\%$ **Eq. 11**

These damping values need to be combined in some form to obtain system damping for the equivalent SDOF structure. A weighted average may be computed as given by

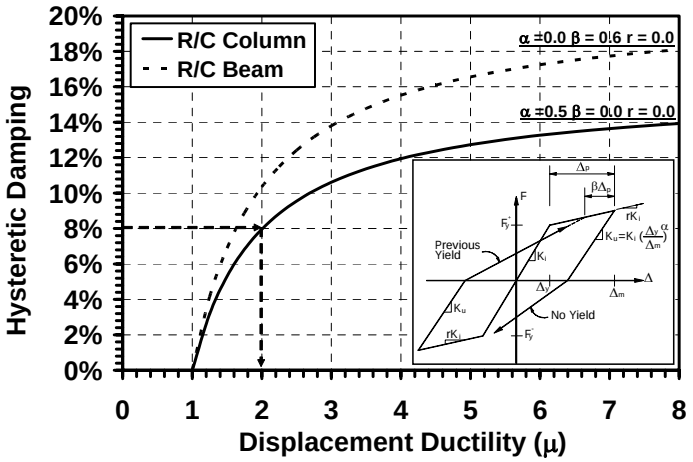

Figure 11 Hysteretic Damping Relation for Takeda's Hysteretic Model

Eq. 12 where Q_i is a weighting factor. Three different approaches have been suggested to compute the weighting factor; firstly Shibata and Sozen [4] suggested that the weighting factor be estimated based on flexural strain energy, secondly, Kowalsky [5] [6] proposed that the factor be based on the work done by each column, and thirdly, Priestley and Calvi [15] proposed that the weighting factor be based on the shear force carried by each member. For the case of a rigid displacement pattern and as a starting point for the case of a flexible pattern, the bridge columns are assumed to have equal reinforcement, as a result column base moments will be equal and shear forces will be inversely proportional to column heights [6] (assuming all columns yield). Consequently, the weighing factor given by Eq. 13 could be used, where h_i is the column height. In the case where some columns remain elastic, the weighting factor for these columns is given by Eq. 14 where μ_i is the displacement ductility. Note that in Eq. 14, the displacement ductility of elastic columns is less than one. In the case where a portion of the seismic forces is resisted by elastic bending of the superstructure, abutment reactions should be included in Eq. 12. In proceeding

iterations, the system damping is computed in proportion to the forces obtained from structural analysis.

$$\xi_{sys} = \sum_i \left(\frac{Q_i}{\sum Q_i} \xi_i \right) \qquad \textbf{Eq. 12}$$

Yielded Columns: $Q_i = 1/h_i$ **Eq. 13**

Elastic Columns: $Q_i = \mu_i / h_i$ **Eq. 14**

5. **Determine Effective Period of the Equivalent Structure**: Utilizing the system target displacement, level of system damping and elastic response spectra for the chosen seismic demand, the effective period of the equivalent structure is determined as shown in Figure 12. For a design displacement of 0.50m and 10% level of equivalent viscous damping, the effective period is estimated to be 3.0 seconds. Once the effective period has been determined, effective stiffness and design base shear are computed by Eq. 15 and Eq. 16, respectively.

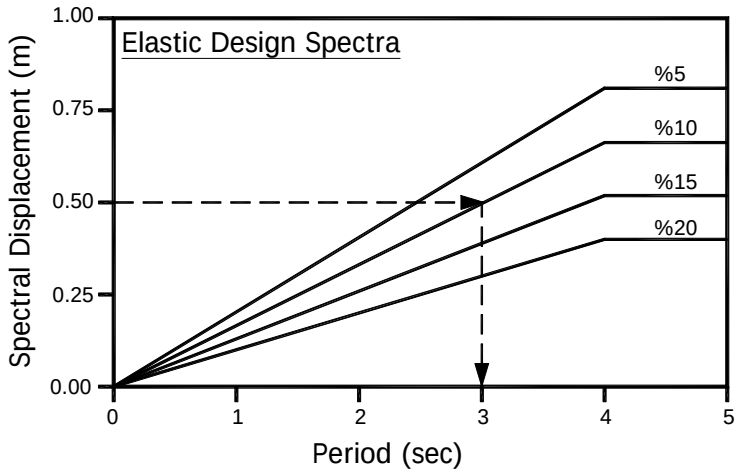

Figure 12 Effective Period Evaluation Based on DDBD Procedure

$$K_{eff} = 4\pi^2 \frac{M_{sys}}{T_{eff}^2} \qquad \textbf{Eq. 15}$$

$$V_B = K_{eff} \Delta_{sys} \qquad \textbf{Eq. 16}$$

6. **Check Design Assumptions**: Distribute the design base shear in proportion to the height inverse as discussed in step 4. Compute the actual initial and secant stiffnesses and recalculate the bridge relative stiffness. If the assumption of a rigid displacement pattern is still valid go to step 8, otherwise, utilize the computed secant stiffnesses in the *effective mode shape* method to obtain a revised flexible target-displacement profile.

7. **Structural Analysis**: Once the target-displacement profile stabilizes, distribute the base shear as inertia forces to the masses of the MDOF structure in accordance with the target-displacement profile as given by Eq. 17 [3]. In this equation F_i are the bent inertia forces, V_B is the design base shear, index i refers to bent number and n is number of bents. Perform structural analysis on the bridge under the inertia loads to obtain the design base shear for each column. Secant stiffnesses should be used in the structural model analysis in order to be consistent with the DDBD philosophy. At this stage of the design column secant stiffnesses are unknown, so as a start, designers should assume reasonable values, conduct the analysis and check the displacement of the critical column (the first column to reach its limit state), if it does not equal the design displacement then the stiffnesses are changed accordingly, and the process is repeated until convergence is achieved.

$$F_i = V_B(m_i\Delta_i)/\sum_{i=1}^{n}(m_i\Delta_i) \qquad \textbf{Eq. 17}$$

In the first structural analysis iteration, it is suggested to distribute the base shear to the columns as given by Eq. 18 where μ_i is less than one for elastic columns and equal to one for columns that have yielded. Secant stiffnesses are then calculated according to Eq. 19 and used in the structural analysis. In Eq. 18 F_{Abt} is the portion of seismic forces carried by abutments, which is assumed to be 30% in the first design iteration and revised according to the structural analysis results.

$$V_i = (V_B - F_{Abt}) \times (\mu_i / h_i)/\sum_{i=1}^{n}\mu_i / h_i \qquad \textbf{Eq. 18}$$

$$(K_{eff})_i = V_i / \Delta_i \qquad \textbf{Eq. 19}$$

Once the displacement profile obtained from structural analysis converges to the assumed target-displacement profile, column secant stiffnesses and abutment forces are compared to assumed values. If the values differ significantly then revise the target-displacement profile utilizing the *effective mode shape* method and structural analysis forces. Repeat steps 3 through 7, skipping step 6, until column secant stiffnesses and abutment forces converge.

8. **Design the MDOF Structure**: Design the structure in accordance with capacity design principles such that the desired failure mechanism is achieved. Further information on the Direct Displacement-Based Design approach can be found in Priestley *et al.* [12].

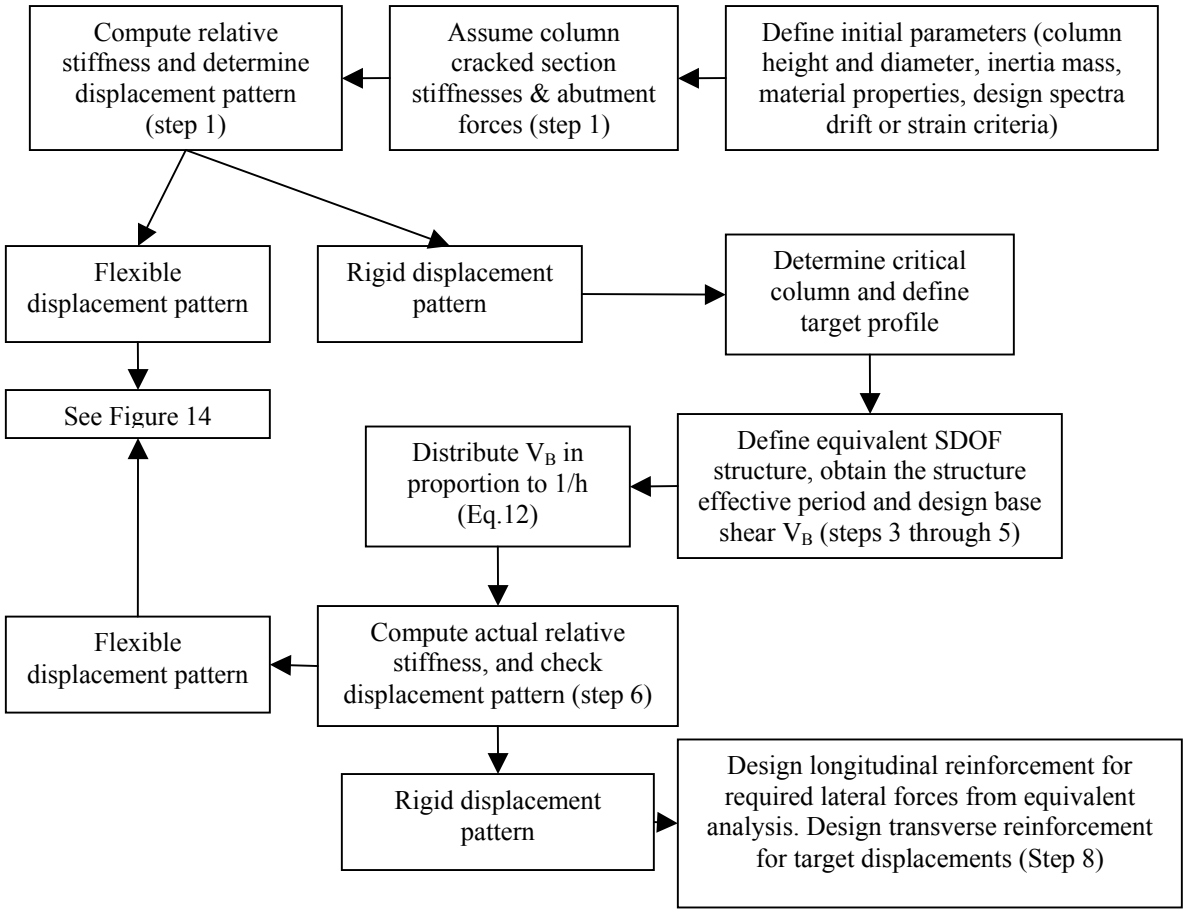

Figure 13 Direct Displacement-Based Design, Part I

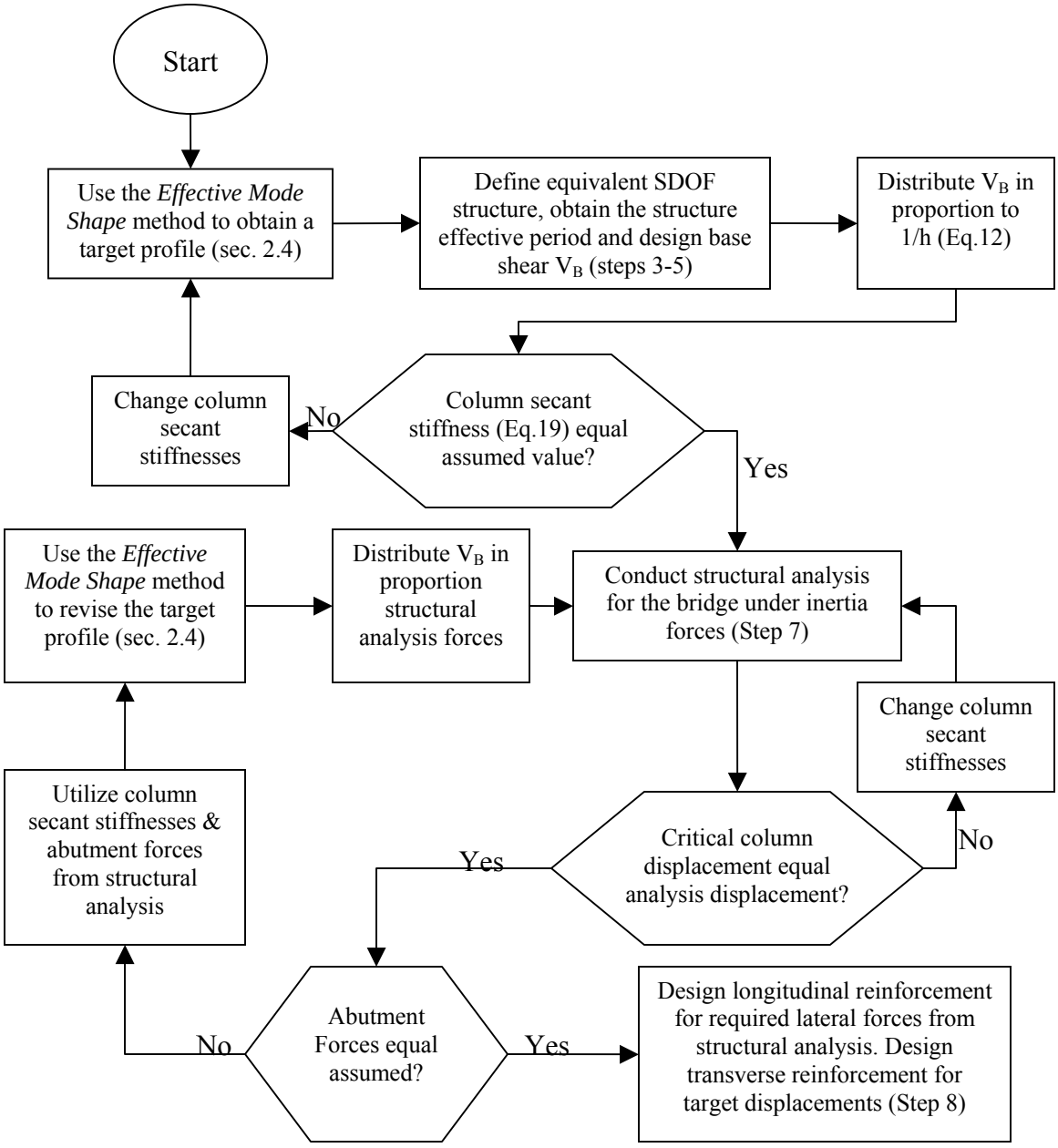

Figure 14 Direct Displacement-Based Design, Part II

4. SAMPLE BRIDGE DESIGNS

The DDBD procedure described by the previous flow charts was applied to a series of bridge structures. Each of the bridges was designed for a drift ratio of 3%. The weight per unit length of the superstructure is 200KN/m (including cap beam). Column heights are measured to the center of the superstructure depth and were assumed to be fixed at the foundation level

and monolithically connected to the superstructure. All steel was assigned a yield stress 455MPa, while concrete compressive strength was 35MPa. The elastic modulus of all concrete was 33.7GPa. The design elastic spectra from *IBC 2000* [16] with PGA of 0.7g were generated for various levels of damping as shown in Figure 15.

The first example (section 4.1) is a 4 span bridge that was designed for a rigid body translation target profile. The second example (section 4.2) consists of a set of 4 bridges with flexible target profiles. One of the 4 bridges is designed in detail, while a summary of the rest of the designs is provided. The third example (section 4.3) is a set of six- and eight- span bridges that were designed with DDBD in order to challenge the design algorithm.

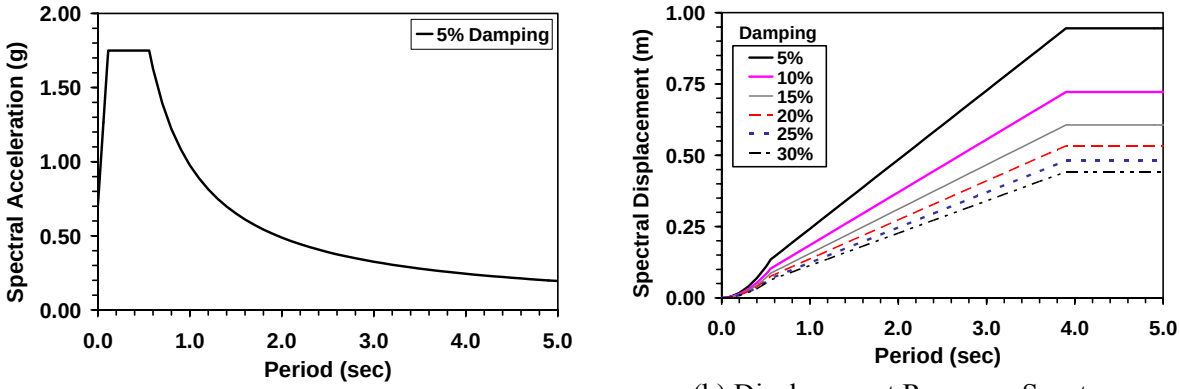

(a) Acceleration Response Spectrum

(b) Displacement Response Spectra

Figure 15 IBC-2000 Soil Type C, 0.7 PGA Response Spectra: (a) Acceleration Response Spectrum, (b) Displacement Response Spectra

4.1 Symmetric Bridge with Rigid Body Translation Target Profile

The first bridge considered in this study is shown in Figure 16. The bridge has a superstructure second moment of area of $100m^4$ and does not have abutment restraint in the transverse direction. The target-displacement profile is determined based on a limit state defined by 3% drift. As a start, a column diameter of 2.0m is assumed which allows calculation of the yield curvature with Eq. 8 and the relative stiffness with Eq. 1. Assuming the column cracked moments of inertia to be 60% of the gross moment of inertia, the bridge relative stiffness (RS) is computed as follow:

***Relative Stiffness*:** $RS = (8/3)(100/140^3)(2 * 8^3/0.471 + 16^3/0.471) = 1.06$

Based on the results shown in Figure 7d and a relative stiffness of 1.06, this bridge is expected to deflect in a rigid body translation mode, where all column displacements are the same. As a result, the shortest column will control the target-displacement profile of the bridge (0.03*8 = 0.24m) as shown in Figure 17. Once the target-displacement profile has been established, the equivalent SDOF structure is defined as follows:

***System Displacement*:** $\Delta_{sys} = 0.24m$

***System Mass*:** $M_{sys} = 140*200/9.805 = 2{,}856KN/g$ (100% of total mass)

Yield Curvature: $\phi_y = 2.25\varepsilon_y/D = 2.25(0.00228/2.0) = 0.00256/m$

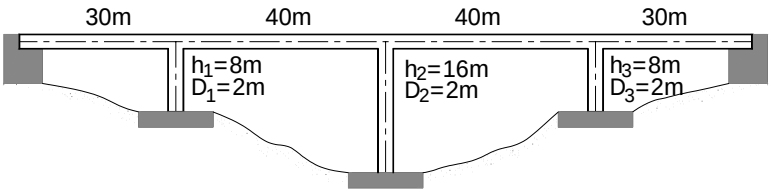

Figure 16 Symmetric Multi-Span Bridge with Free Abutments

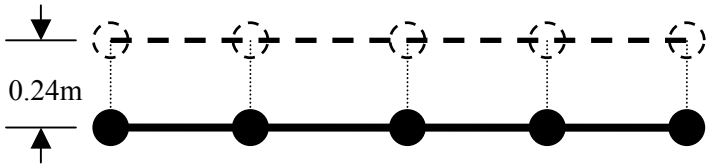

Figure 17 Presumed Target-Displacement Profile

For the purposes of yield displacement calculation, a strain penetration of $0.022f_yd_b = 0.022*455*0.042 = 0.42m$ is added to the column heights. Thus the yield displacements are:

$\Delta_{y1} = \Delta_{y3} = 0.00256*8.42^2/3 = 0.06m$; $\Delta_{y2} = 0.00256*16.42^2/3 = 0.23m$.

***Displacement Ductilities*:** $\mu_1 = \mu_3 = 0.24/0.06 = 4$; $\mu_2 = 0.24/0.23 = 1.04$

***Column Equivalent Damping*:** Assuming a 2% elastic damping and utilizing Eq. 10, the equivalent damping is computed as follow:

$\xi_1 = \xi_3 = 2 + (50/3.14)(4 - 1)/4 = 14\%$
$\xi_2 = 2 + (50/3.14)(1.06 - 1)/1.06 = 3\%$

***System Damping*:** Equal reinforcement is selected for all columns. Consequently, base moments are also equal and column base shear is inversely proportional to column height (since all columns yield). Thus, system damping is computed in accordance with Eq. 12 and Eq. 13:

$$\xi_{sys} = (0.4*14 + 0.2*3 + 0.4*14) = 11.8\%$$

***Effective Period*:** According to *EuroCode 8* [17], the spectral displacement reduction factor for the computed system damping is $(7/(2+11.8))^{0.5} = 0.712$. Reducing the 5% displacement design spectra and entering with the system displacement, the effective period of the equivalent structure is found to be **1.38sec**.

***Effective Stiffness*:** $K_{eff} = 4\pi^2 M_{sys}/(T_{eff})^2 = 4\pi^2(28{,}000/9.805)/1.38^2 = 59{,}200$KN/m.

***Base Shear*:** $V_B = K_{eff}\,\Delta_{sys} = 59.2 * 0.24 = 14{,}208$KN.

Distribute the base shear to the columns in proportion to 1/h, which is consistent with the basic assumption of equal reinforcement:

$$V_{B1} = V_{B3} = 0.4 * 14.208 = 5{,}683\text{KN} \; ; \; V_{B2} = 0.2 * 14.21 = 2{,}842\text{KN}.$$

***Check Basic Assumptions*:** Compute the actual cracked section moments of inertia and revise the estimated relative stiffness. Since the bilinear factor for Takeda's model used in the design equals 0.0, the yield moment is equal to the ultimate moment. As a result, the actual cracked section moments of inertia are:

$I_{cr1} = I_{cr3} = ((5.683*8)/(33.7*10^3 * 0.00256) = 0.527m^4$ (67% of I_g)
$I_{cr2} = ((2.842*16)/(33.7*10^3 * 0.00256) = 0.527m^4$ (67% of I_g)
Consequently, RS = 0.95 (insignificant change in RS value, which was originally estimated as 1.06)

***Design Verification*:** In order to verify the previous design in terms of meeting the target-displacement profile and hence damage levels, the bridge was subjected to 4 artificially generated earthquakes through inelastic time history analysis. The analyses were performed with RUAUMOKO [9], using the Takeda hysteretic model shown in Figure 11 for R/C columns to model the pier inelastic action. The artificial earthquakes were generated with the computer program *SIMQKE* [18] to fit the design spectrum. However a certain amount of scatter in the artificial records and their associated response spectra is expected. Bridge

columns were modeled as inelastic members with design yield strength and cracked section moments of inertia, while the superstructure was modeled as an elastic member.

Shown in Figure 18 are maximum displacements from inelastic time history analysis with the design target profile. Clearly, the analysis results match the design profile reasonably well and also confirm the assumption of a rigid body translation displacement pattern.

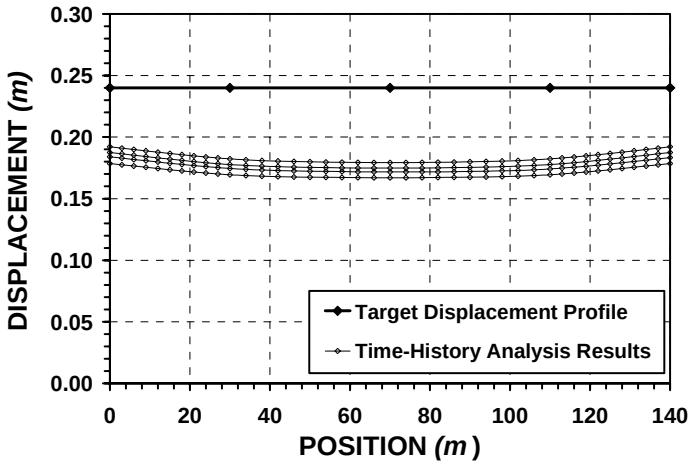

Figure 18 Time History Analysis Results – Symmetric Bridge with Rigid Body Translation Target Profile

4.2 Bridges with Flexible Target Displacement Profiles

Under this category, a series of 4 multi-span bridge structures, as shown in Figure 19, were designed for a 3% drift limit state under the design spectra shown in Figure 15. Only the design of one asymmetric bridge, shown in Figure 19d, will be discussed in detail. Further information on the design of the other bridges can be found in Dwairi [19]. Each of the 4 bridges was designed with abutments integrally built to the superstructure. Abutments were assumed to be fully restrained against translational movement in the transverse direction. All bridge superstructures have a moment of inertia about the vertical axis equal to $50m^4$.

- *Detailed Design of BR8-16-24*

Since this bridge is expected to have a flexible displacement pattern, the *effective mode shape* method described in section 2.4 is used to determine the target displacement profile. A 2.5m

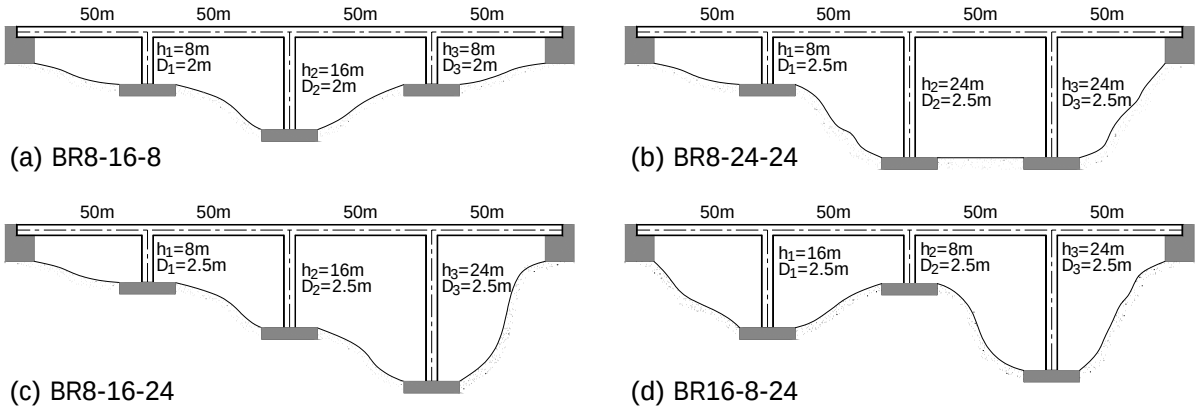

Figure 19 Bridge Configurations Considered for the Design of Flexible Scenarios

column diameter was selected. As a first estimate, assume the secant stiffness of all columns to be equal to 10% of the uncracked stiffness (K_g) and solve the eigenvalue problem. Considering the first three mode shapes and following the Effective mode shape method steps, the following displacement pattern was obtained: $\delta_1 = 0.338$, $\delta_2 = 0.623$ and $\delta_3 = 0.520$. For this pattern and a drift limit of 3%, the shortest column was determined to be the critical column. Thus, scaling the displacement pattern so that the shortest column has a displacement of 0.03*8 = 0.24m results in the following target-displacement profile: $\Delta_1 = 0.240$m and $\Delta_2 = 0.442$m and $\Delta_3 = 0.369$m. Once the target profile has been established, the equivalent SDOF structure is defined as follow:

System Displacement: The superstructure is modeled with 5 nodes, two of which are pinned and have no contribution to the work done by the structure. The masses at the top of the piers are: $m_1 = m_2 = m_3 = 50*200/9.805 = 1{,}020$KN/g. The system displacement is computed according to Eq. 6:

$$\Delta_{sys} = (0.24^2 + 0.442^2 + 0.369^2)/(0.24 + 0.442 + 0.369) = 0.370\text{m}$$

System Mass: The equivalent SDOF structure mass is computed in accordance with Eq. 7:

$$M_{sys} = 1{,}020*(0.24 + 0.442 + 0.369)/0.370 = 2{,}895\text{KN (94.7\% of participating mass)}$$

Yield Curvature: $\phi_y = 2.25\varepsilon_y/D = 2.25(0.00228/2.5) = 0.00205$/m

Yield Displacements: Adding 0.42m strain penetration to column heights, the column yield displacements will be:

$\Delta_{y1} = 0.00205*8.42^3/3 = 0.048m$; $\Delta_{y2} = 0.00205*16.42^3/3 = 0.184m$
$\Delta_{y3} = 0.00205*24.42^3/3 = 0.407m$

Displacement Ductilities: $\mu_1 = 0.24/0.048 = 5$; $\mu_2 = 0.442/0.0.184 = 2.40$
$\mu_3 = 0.369/0.407 = 0.905$ (elastic)

Column Equivalent Damping: Utilizing Eq. 10 and adding 2% viscous damping, the following equivalent damping values are computed:

$\xi_1 = 2 + (50/3.143)(5 - 1)/5 = 14.7\%$
$\xi_2 = 2 + (50/3.143)(2.40 - 1)/2.40 = 11.3\%$
$\xi_3 = 2\%$

System Damping: Since at this stage in the design we do not know the inertia forces carried by the abutments due to elastic bending of the superstructure, we make an assumption that 30% of the total shear is carried by the abutments with a damping value of 5%. System damping is then calculated in proportion to the shear force carried by each member according to Eq. 12 and Eq. 14, assuming equal reinforcement in the columns. Thus, the weighting factors and system damping are calculated as follow:

$\sum \mu_i / h_i = (1/8) + (1/16) + (0.905/24) = 0.225$
$Q_1 = 0.7*(1/8)/0.225 = 0.388$
$Q_2 = 0.7*(1/16)/0.225 = 0.194$
$Q_3 = 0.7*(0.905/24)/0.225 = 0.117$
$\xi_{sys} = (0.3*5 + 0.388*14.7 + 0.194*11.3 + 0.117*2) = 9.60\%$

***Effective Period*:** According to *EuroCode 8* [17], the spectral displacement reduction factor for the computed system damping is $(7/(2+9.6))^{0.5} = 0.777$. Reducing the 5% displacement design spectra shown in Figure 15b and entering with system displacement of 0.370m, the effective period of the equivalent structure is found to be **1.97 seconds**

Effective Stiffness: $K_{eff} = 4*(3.143)^2*2,895/1.97^2 = 29,489KN/m$

Base Shear: $V_B = 29.489*0.287 = 10,918KN$

Recall that 30% of total force is carried by the abutments and equal base moment for all columns was assumed in the design, based on that the base shear is distributed as follow:

$V_{B1} = 0.388*10.918 = 4,241KN$
$V_{B2} = 0.194*10.918 = 2,121KN$

V_{B3} = 0.117*10.918 = 1,281KN

Now, the primary assumption that all columns have secant stiffnesses equal to 10% of the uncracked stiffness is checked. The secant stiffnesses and effective moments of inertia are computed according to Eq. 20 and Eq. 21 as follow:

$$K_{eff} = V_B / \Delta \qquad \textbf{Eq. 20}$$

$$I_{eff} = (K_{eff} h^3) / (3E_c) \qquad \textbf{Eq. 21}$$

K_{eff1} = 4,141/0.240 = 17,671KN/m ; K_{eff2} = 2,121/0.442 = 4,796KN/m
K_{eff3} = 1,281/0.369 = 3,473KN/m
I_{eff1} = 17,671*8^3/(3*33.7*10^6) = 0.089m^4 (4% of I_g)
I_{eff2} = 4,796*16^3/(3*33.7*10^6) = 0.194m^4 (8.7% of I_g)
I_{eff3} = 3,473*24^3/(3*33.7*10^6) = 0.475m^4 (21.2% of I_g)

Because of the difference between the assumed secant stiffnesses and computed stiffnesses, a second iteration is needed. The second iteration results are shown in Table 2. Clearly, there is still some difference between assumed and calculated stiffness values. Two additional iterations were carried out until the target-displacement profile stabilized. The results from the last iteration are also shown in Table 2.

Table 2 Summary of Design Iterations (Abt. force = 30% of total shear)

Item	Abut.1	Column1	Column2	Column3	Abut.2
	SECOND ITERATION				
Computed Secant Stiffness, $K_{eff.}$		4.0%K_{g1}	8.7%K_{g2}	21.2%K_{g3}	
	REVISED TARGET DISPLACEMENT PROFILE				
Target Profile (m)	0	0.240	0.378	0.2870	0
System Displacement. (m)	0.313				
System Mass (KN/g)	2,953				
Displacement Ductility		5.0	2.05	0.706	
Equivalent Damping		14.7%	10.2%	2.0%	
System Damping	10.0%				
Effective Period, T_{eff} (sec)	1.70				
Equivalent SDOF K_{eff} (KN/m)	41,410				
Design Base Shear (KN)	12,946				
	SHEAR FORCE DISTRIBUTION				
Assigned Base Shear (KN)		5,222	2,611	1,229	
Computed Secant Stiffness		4.9%K_{g1}	12.9%K_{g2}	26.1%K_{g3}	
	FOURTH ITERATION				
Computed Secant Stiffness, $K_{eff.}$		4.6%Kg1	11.5%Kg2	24.6%Kg3	
	REVISED TARGET DISPLACEMENT PROFILE				
Target Profile (m)	0	0.240	0.384	0.296	0
System Displacement. (m)	0.318				
System Mass (KN/g)	2,950				

Table 2 Continue …

Item	Abut.1	Column1	Column2	Column3	Abut.2
Displacement Ductility		5.0	2.09	0.726	
Equivalent Damping		14.7%	10.3%	2.0%	
System Damping	10.1%				
Effective Period, T_{eff} (sec)	1.73				
Equivalent SDOF K_{eff} (KN/m)	39,120				
Design Base Shear (KN)	12,436				
	SHEAR FORCE DISTRIBUTION				
Assigned Base Shear (KN)		4,997	2,499	1,210	
Computed Secant Stiffness, K_{eff}		$4.7\%K_{g1}$	$11.8\%K_{g2}$	$24.9\%K_{g3}$	

After the target displacement profile has been established, structural analysis is conducted to determine the actual force carried by members. Design base shear is distributed to the masses at the top of the columns in accordance with Eq. 17. The inertia forces are:

$F_1 = 12{,}436*(1.02*10^6*0.24)/9.377*10^5 = 3{,}246KN.$
$F_2 = 12{,}436*(1.02*10^6*0.384)/\ 9.377*10^5 = 5{,}191KN.$
$F_3 = 12{,}436*(1.02*10^6*0.296)/\ 9.377*10^5 = 3{,}999KN$

The structure is then analyzed under the previous inertia forces utilizing the secant stiffnesses from the last iteration, see Table 2. The displacement of the critical column is compared with the corresponding target displacement, if both values differ, the column stiffnesses are changed accordingly and the analysis is repeated until convergence is achieved. The results from the structural analysis are shown in Table 3.

Table 3 Summary of Structural Analysis

Item	Abut.1	Column1	Column2	Column3	Abut.2
	FIRST ITERATION				
Assigned Base Shear (KN)		4,997	2,499	1,210	
Analysis Displacement (m)	0	0.229	0.367	0.283	0
Analysis Base Shear (KN)	971	4,766	2,389	1,158	3,152
	SECOND ITERATION				
Assumed Base Shear (KN)		4,766	2,383	1,154	
Analysis Displacement (m)	0	0.237	0.378	0.290	
Analysis Base Shear (KN)	1,049	4,701	2,345	1,132	3,210
Computed Secant Stiffness, K_{eff}		$4.4\%K_{g1}$	$11\%K_{g2}$	$23.3\%K_{g3}$	
	CONVERGENCE ACHIEVED				

Note that the forces carried by the abutments are 34.2% of the total design shear force which is 4.2% greater than the assumed value. Although this difference is not expected to cause a significant change in the target profile, the *effective mode shape* method is used once again with the secant stiffness values and abutment forces based on the structural analysis

results. The results are shown in Table 4. Finally, conduct structural analysis utilizing member effective properties to distribute the design base shear (12,676KN) to the members. A summary of the analysis results is shown in Table 5. Since abutment reactions and column effective stiffnesses did not change from what was assumed, the design was concluded.

The design results for all the bridges, shown in Figure 19, are presented in Table 6. Note that the number of iterations required to achieve convergence increases with the degree of bridge irregularity. Also in all design cases, the shortest column controlled the amplitude of the target deflection profile. BR16-8-24 has the smallest system displacement of 0.203m, and the shortest effective period, as well. Abutment forces ranged between 27.1% and 34.1% of the total design shear. The previous designs were verified through inelastic time history analysis. The same verification process described in section 4.1 was followed. The results from the time history analysis with the target displacement profile are shown in Figure 20. Clearly the *effective mode shape* method was able to capture the displacement pattern, reasonably well, for all the bridges.

Table 4 Final Design Iteration

Item	Abut.1	Column1	Column2	Column3	Abut.2
Computed Secant Stiffness, $K_{eff.}$		$4.4\%K_{g1}$	$11\%K_{g2}$	$23.3\%K_{g3}$	
	REVISED TARGET DISPLACEMENT PROFILE				
Target Profile (m)	0	0.240	0.382	0.293	0
System Displacement. (m)	0.316				
System Mass (KN/g)	2,951				
Displacement Ductility		5.0	2.07	0.72	
Equivalent Damping		14.7%	10.2%	2.0%	
System Damping	10.0%				
Effective Period, T_{eff} (sec)	1.71				
Equivalent SDOF K_{eff} (KN/m)	40,1000				
Design Base Shear (KN)	12,676				
	SHEAR FORCE DISTRIBUTION				
Assigned Base Shear (KN)		4,791	2,390	1,154	
Computed Secant Stiffness, K_{eff}		$4.5\%K_{g1}$	$11.3\%K_{g2}$	$24.0\%K_{g3}$	

Table 5 Distribution of Final Design Base Shear

Item	Abut.1	Column1	Column2	Column3	Abut.2
Assigned Base Shear (KN)		4,791	2,390	1,154	
Analysis Displacement (m)	0	0.240	0.383	0.294	0
Analysis Base Shear (KN)	1,065	4,798	2,401	1,160	3,252
	CONVERGENCE ACHIEVED				

Table 6 Summary of Design Results for 4 Flexible Superstructure Bridges

Item	BR8-16-8	BR8-24-24	BR8-16-24	BR16-8-24
Top of Pier 1 Target Disp. (m)	0.240	0.240	0.240	0.163
Top of Pier 2 Target Disp. (m)	0.349	0.396	0.382	0.240
Top of Pier 3 Target Disp. (m)	0.240	0.307	0.293	0.190
System Displacement (m)	0.286	0.328	0.316	0.203
System Mass/Total Mass (%)	96.6	96.0	96.5	97.5
System Damping (%)	11.0	8.9	10.0	8.8
Effective Period (sec)	1.61	1.68	1.71	1.04
Abutment 1 Reaction (KN)	1,757	718	1,065	2,251
Pier 1 Base Shear (KN)	3,773	5,893	4,798	4,338
Pier 2 Base Shear (KN)	1,885	1,910	2,401	9,812
Pier 3 Base Shear (KN)	3,773	1,479	1,160	1,530
Abutment 2 Reaction (KN)	1,757	3,402	3,252	4,162
Abutment Force/Total Shear (%)	27.1	30.7	34.1	29.0
Number of Design Iterations	3	4	4	4

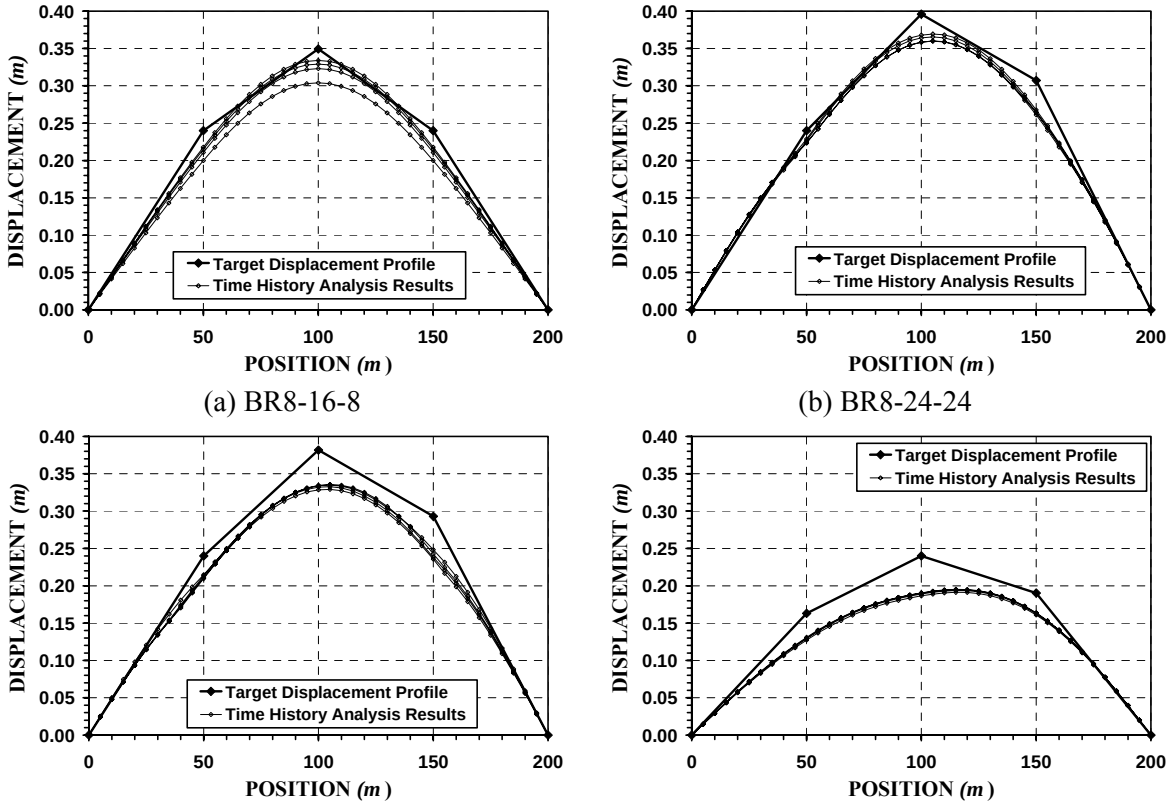

(a) BR8-16-8 (b) BR8-24-24

(c) BR8-16-24 (d) BR16-8-24

Figure 20 Maximum Displacements from Time History Analysis – Flexible Superstructure Bridges.

4.3 Six- and Eight- Span Bridge Designs

In this category, the design algorithm shown in Figure 13 was challenged by applying it to 2 six-span and 2 eight-span bridge structures as shown in Figure 21. A relatively stiff superstructure with a moment of inertia about the vertical axis equal to $85m^4$ was used. A column diameter of 2.5m was selected for all 4 bridges. Each bridge was to be designed for 3% drift under the design spectra shown in Figure 15. The design results are summarized in Table 7.

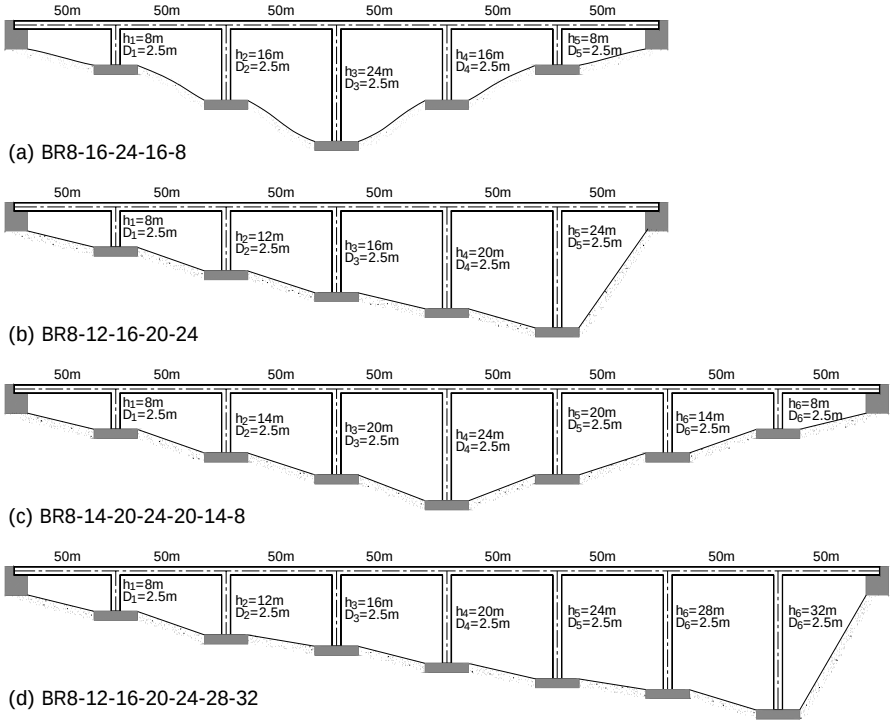

Figure 21 Six- and Eight- Span Bridge Configurations Designed with DDBD

Table 7 Summary of Design Results for Six- and Eight- Span Bridges

Item	BR8-16-24-16-8	BR8-12-16-20-24	BR8-14-20-24-20-14-8	BR8-12-16-20-24-28-32
Top of Pier 1 Target Disp. (m)	0.240	0.179	0.215	0.178
Top of Pier 2 Target Disp. (m)	0.439	0.357	0.420	0.332
Top of Pier 3 Target Disp. (m)	0.522	0.480	0.587	0.480
Top of Pier 4 Target Disp. (m)	0.439	0.462	0.656	0.592
Top of Pier 5 Target Disp. (m)	0.240	0.286	0.587	0.609
Top of Pier 6 Target Disp. (m)	N/A	N/A	0.420	0.510
Top of Pier 7 Target Disp. (m)	N/A	N/A	0.215	0.298
System Displacement (m)	0.411	0.388	0.505	0.481
System Mass/Total Mass (%)	91.4	90.8	87.7	89.1

Table 7 Continue …

Item	BR8-16-24-16-8	BR8-12-16-20-24	BR8-14-20-24-20-14-8	BR8-12-16-20-24-28-32
System Damping (%)	12.2	10.2	11.8	8.7
Effective Period (sec)	2.414	2.118	2.925	2.454
Abutment 1 Reaction (KN)	537	799	735	53.8
Pier 1 Base Shear (KN)	3,546	4,479	3,300	1,331
Pier 2 Base Shear (KN)	1,814	3,399	2,296	3,001
Pier 3 Base Shear (KN)	1,204	2,633	1,725	3,668
Pier 4 Base Shear (KN)	1,814	2,155	1,442	3,393
Pier 5 Base Shear (KN)	3,546	1,266	1,725	3,133
Pier 6 Base Shear (KN)	N/A	N/A	2,296	2,684
Pier 7 Base Shear (KN)	N/A	N/A	3,300	1,050
Abutment 2 Reaction (KN)	537	2,713	735	1,863
Abutment Force/Total Shear (%)	8.3	20.1	8.4	9.6
Number of Design Iterations	4	7	6	11

The previous designs were verified through inelastic time history analysis under the same 4 artificial earthquakes used in the previous examples. The maximum displacements from time history analysis with target design profiles are shown in Figure 22. Clearly, there is good agreement between target-displacement profiles and analysis results.

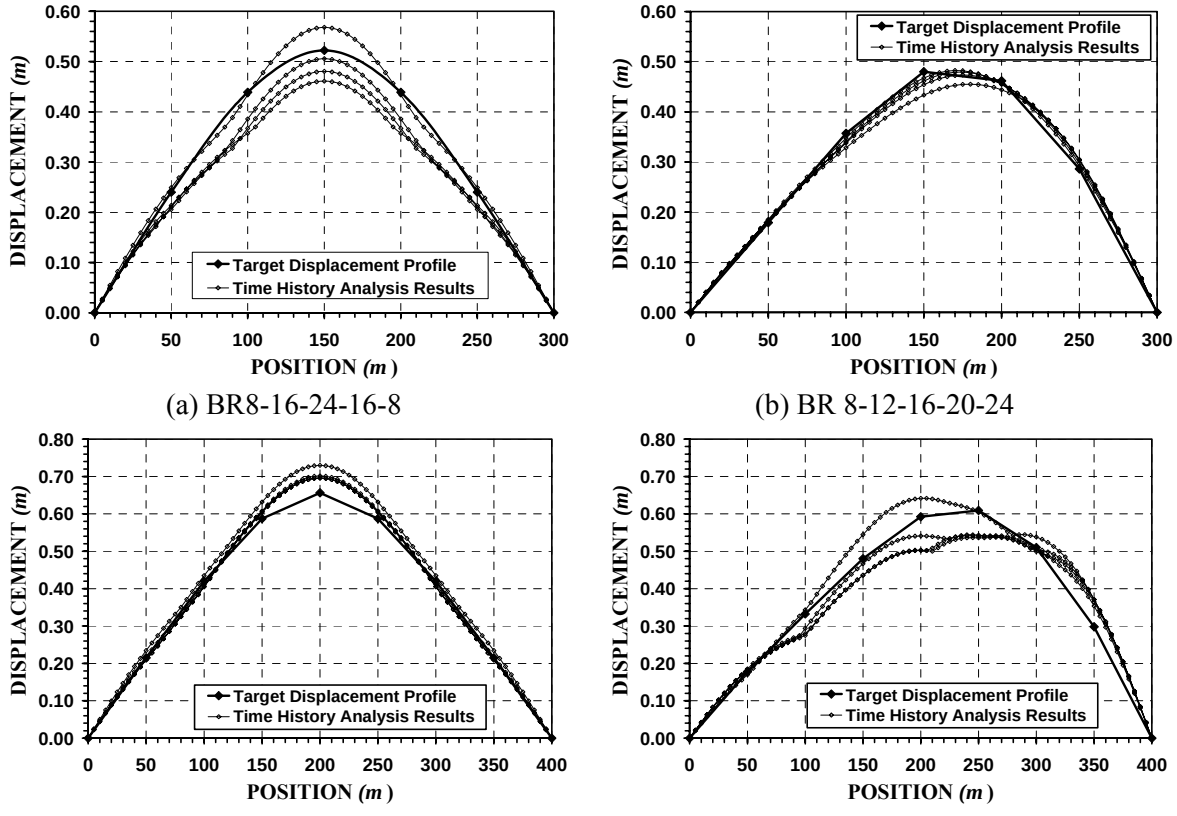

(a) BR8-16-24-16-8 (b) BR 8-12-16-20-24

(c) BR 8-14-20-24-20-14-8 (d) BR 8-12-16-20-24-28-32

Figure 22 Maximum Displacements from Time History Analysis – 6 and 8 Span Bridges

5. EVALUATION OF DDBD FOR MULTI-SPAN BRIDGES

In order to evaluate the accuracy of DDBD procedure to predict the target-displacement profile, 100 bridge design cases were carried out and verified through inelastic time history analysis. Parameters considered in the study included bridge geometry as shown in Table 8, superstructure stiffness and design spectra. Each bridge was designed for superstructure moments of inertia equal to $50m^4$ and $100m^4$. The spectra shown in Figure 15 were used twice in the design with peak ground acceleration (PGA) equal to 0.7g and 1.0g. A limit state that corresponds to 3% drift was considered in the designs.

Table 8 Bridge Configurations

Symmetric Bridges	Asymmetric Bridges
BR8-8-8	BR8-16-16
BR8-16-8	BR8-24-24
BR16-8-16	BR8-16-24
BR8-16-16-8	BR16-8-24
BR16-8-8-16	BR8-24-16
BR8-8-8-8	BR8-16-24-32
BR8-16-24-16-8	BR16-8-32-24
BR16-8-24-8-16	BR8-14-20-24-30
BR8-16-24-24-16-8	BR8-14-30-24-20
BR16-8-24-24-8-16	BR8-16-24-32-20-10
BR8-16-24-32-24-16-8	BR8-8-16-16-24-24
BR16-8-24-32-24-8-16	BR8-12-16-20-24-28-32
BR16-24-8-32-8-24-16	BR12-8-16-32-28-24-20

The bridges were subjected to 4 artificial earthquakes that fit the design spectra. The maximum displacements from the NLTH analyses were averaged and compared to the target displacements. Figure 23 shows the ratio of the NLTH displacements to target displacements plotted against column positions across the bridge normalized to the bridge total length. Each line represents the average analysis results for one bridge. Clearly, for 4 and 5 span bridges the NLTH displacements (Δ_{NLTH}) were somewhat less than the design target displacements (Δ_{Target}). The DDBD procedure was reasonably accurate in predicting the bridge target-displacement profile, which is implied by the almost uniform ratios across the bridge as shown in Figure 23a. On the other hand, the NLTH displacements exceeded the target displacements in about half of the 6, 7 and 8 spans cases presented in Figure 23b and

apparently the design algorithm failed in some of the cases to select a target profile that is compatible with the bridge 'actual' deflected shape.

Similar to the symmetric bridges, Figure 24 shows the ratios of the NLTH displacements to target displacements against column positions normalized to bridge total length for asymmetric group of bridges. The ratios of NLTH to target displacements for the cases of 4 and 5 span bridges were evenly distributed about 1, and in most of the cases the displacement profile was predicted with a reasonable accuracy. However, for bridges with 6, 7 and 8 spans as shown in Figure 24b, target displacements were exceeded in the majority of the cases. The DDBD procedure failed to select a target profile that is compatible with the bridge 'actual' deflected shape in about 30% of the 6, 7 and 8 span design cases.

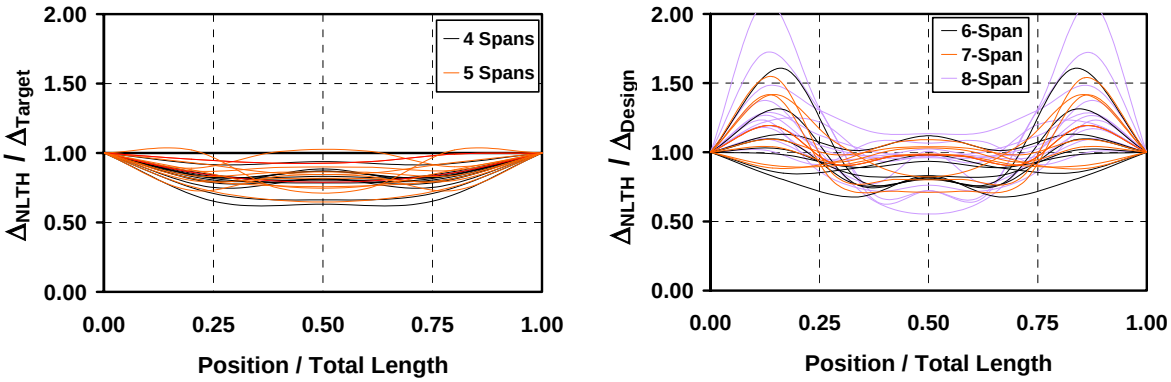

(a) 4 and 5 Span Design Cases (b) 6, 7 and 8 Span Design Cases

Figure 23 Nonlinear Time History Analysis to Target Displacement Ratios for Symmetric Bridges: (a) 4 and 5 Span Design Cases (b) 6, 7 and 8 Span Design Cases.

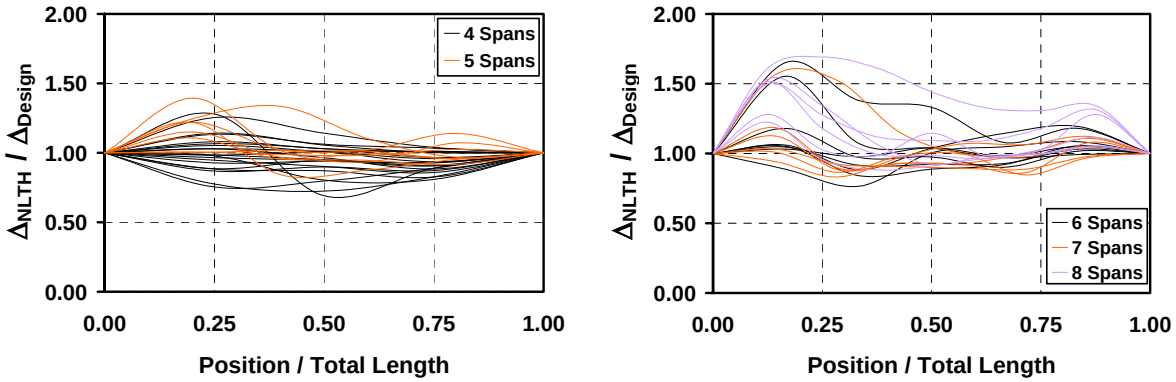

(a) 4 and 5 Span Design Cases (b) 6, 7 and 8 Span Design Cases

Figure 24 Nonlinear Time History Analysis to Target Displacement Ratios for Asymmetric Bridges: (a) 4 and 5 Span Design Cases (b) 6, 7 and 8 Span Design Cases.

It is important to note that the ratios shown in the previous figures do not exactly represent the ratio of the 'actual' deflected shape to the target profile displacements; they actually represent the ratios of the NLTH displacements envelope to the target profile. However, in the majority of the design cases, the maximum NLTH displacements occurred at almost the same time, and as a result, the displacements envelope coincided with the actual displacement profile.

In order to shed some light on why the DDBD failed to predict the displacement profile of some of the 6, 7 and 8 span bridges, one of the previous design cases was studied in more detail. Figure 25 shows a comparison between NLTH maximum displacements and target displacements for BR16-24-8-32-8-24-16. The bridge was designed for a 3% drift limit, superstructure moment of inertia equal to $50m^4$ and the design spectra shown in Figure 15 scaled to 0.7g PGA. The dark line (envelope 1) in Figure 25 represents the maximum NLTH displacements of the bridge where member shear forces were obtained based on structural analysis under inertia forces as discussed in section 4. Clearly, the effective modal analysis (using secant stiffness at maximum response), which forms the basis of the target displacement profile, and shear forces distribution do not match the NLTH analysis. For a nonlinear SDOF system, the structure may be represented with equivalent linear system that is defined by the secant stiffness at peak response and equivalent damping based on the amount of energy dissipated. However, for a MDOF system, damping values less than 20% have insignificant effect on the mode shapes and damped frequencies [20], which is why the modal analysis using effective properties of the structure will not yield a correct target-displacement profile unless the response is dominated by the first mode. Therefore, in Figure 25 the design assumed that the two shortest columns will yield, while the NLTH analysis revealed that four columns actually yielded with different levels of ductility from that which the design procedure anticipated. Despite the inaccuracy in the chosen target profile, the design base shear was redistributed to the columns based on NLTH analysis. In this procedure, column shear forces were assumed and displacements from NLTH were compared to the corresponding target displacements, if they differ, column strengths were changed accordingly until convergence is achieved. After three iterations the NLTH analysis yielded envelope 2, which agrees well with the presumed target profile. Although this

procedure is expected to yield a distribution of shear forces that agrees well with the selected target profile, it is still computationally extensive which negates the idea of a simplified design approach. However, this procedure is only needed for few cases where bridge configurations are abnormal and rarely found in practice.

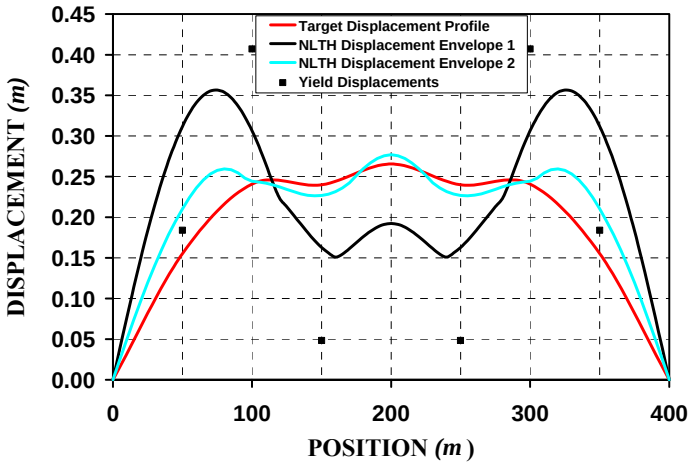

Figure 25 Design Results for BR16-24-8-32-8-24-16

6. CONCLUSIONS

Described in this paper is a study aimed at identifying inelastic displacement patterns for multi-span bridges in support of the direct displacement-based seismic design procedure. Three different displacement patterns were identified, namely: (1) Rigid body translation, (2) Rigid body translation and rotation, and (3) Flexible pattern. These three patterns were found to be highly dependent on the relative stiffness between superstructure and substructure, bridge regularity and abutment type. The first two patterns require minimal effort in the DDBD approach, since no iterations are required to converge to a target displacement profile. However, the third pattern requires iterating over the target-displacement profile until convergence is achieved.

In order to identify these patterns, a series of nonlinear dynamic time history analyses were conducted on selected multi-span bridges. Variables considered included bridge geometry, superstructure stiffness, substructure stiffness, abutment conditions, column flexural strength, and earthquake time history. Based on the analyses results, a rigid body translation pattern was identified for symmetric bridges with free abutments. In addition, a

rigid body translation with rotation was identified for asymmetric bridges with free abutments. The majority of the bridges with abutment restraint in the transverse direction had flexible displacement patterns with a coefficient of variation of the displacements less than 50%. Three sets of design examples were provided to demonstrate the DDBD approach for rigid body translation and flexible displacement patterns. The design algorithm showed good agreement between design and analysis displacements for most of the design cases. However, some inaccuracy was noticed as the number of spans or bridge irregularity increased.

The DDBD procedure was evaluated for about 100 multi-span bridge design cases. The evaluation process showed that all of the 4 and 5 span symmetric bridge cases had NLTH displacements less than the target displacements and accurately predicted the target-displacement profile. The NLTH to target displacement ratios were evenly distributed around 1 for 4 and 5 span asymmetric bridges with a good accuracy in predicting the target profiles for most of the cases. However, the target displacement were exceeded in over than 50% of the design cases for 6, 7 and 8 span bridges for symmetric and asymmetric configurations. In a limited number of cases with abnormal configurations and flexible superstructures, the design procedure failed to predict the target-displacement profile. The failure is attributed to the inability of the effective modal analysis to estimate the target-displacement profile of a yielding MDOF structure. It is will established that damping values less than 20% have insignificant effect on the mode shapes, therefore, the equivalent damping associated with secant stiffness at peak response of a yielding structure have no effect on the mode shapes and results in inaccurate displacement profile estimates.

7. REFERENCES

1. Kowalsky M.J., Priestley M.J.N. and MacRae G.A., Displacement-based Design of RC Bridge Columns in Seismic Regions, *Earthquake Engineering and Structural Dynamics*; December 1995. pp. 1623-1643

2. Priestly, M.J.N. Myths and fallacies in earthquake engineering – conflicts between design and reality. *Bulletin*, NZ National Society for Earthquake Engineering 1993; **26**(3).

3. Calvi G.M. and Kingsley G.R., Displacement based seismic design of multi-degree-of-freedom bridge structures, *Earthquake Engineering and Structural Dynamics*, December 1995; **24**: 1247-1266.

4. Shibata A. and Sozen M. Substitute structure method for seismic design in R/C. *Journal of the Structural Division*, ASCE 1976; **102**(ST1): 1-18.

5. Kowalsky, M.J. Direct displacement-based design: A seismic design methodology and its application to concrete bridges. *Ph.D. Dissertation*, UCSD, Division of Structural Engineering, June 1997, La Jolla, CA 92093-0085.

6. Kowalsky M.J. A Displacement-based approach for the seismic design of continuous concrete bridges. *Earthquake Engineering and Structural Dynamics* 2002; **31**: 719-747.

7. Kowalsky M.J. Deformation limit states for circular reinforced concrete bridge columns. *Journal of Structural Engineering*, *ASCE*; 2000, **126**(8): 1-10.

8. CALTRANS. Memo to Designers 5-1. *California Department of Transportation, Division of Structures*, Sacramento, CA. 1992.

9. Carr A. *RUAUMOKO Users Manual*. University of Canterbury: Christchurch, New Zealand; 1996.

10. Takeda T., Sozen M. and Nielsen N. Reinforced Concrete Response to Simulated Earthquakes. *Journal of the Structural Division*, ASCE 1970; **96**(12): 2557-2573

11. Jacobsen L.S. Steady Forced Vibrations as Influenced by Damping. *ASME Transactione* 1930; **52**(1): 169-181.

12. Priestley MJN., Calvi G.M. and Kowalsky M.J. Direct Displacement-Based Seismic Design of Structures. *IUSS Press* 2005; Pavia, Italy. In Preparation.

13. Dwairi H.M, Mervyn M.J. and Nau J.M. Equivalent damping in support of direct displacement-based design. *Earthquake Engineering and Structural Engineering*. 2005. (under review)

14. Grant D.N., Blandon C.A. and Priestley M.J.N. Modeling inelastic response in direct displacement-based design. *Report No. ROSE 2004/02*, European School of Advanced Studies in Reduction of Seismic Risk, Pavia, Italy.

15. Priestley M.J.N. and Calvi G.M. Direct displacement-based seismic design of concrete bridges. 5th *International Conference (ACI)*: Seismic Bridge Design and Retrofit for Earthquake Resistance; December 8-9, 2003. La Jolla, California.

16. International Building Code, IBC 2000 – Section 1615: Earthquake loads, Site ground motion. *International Code Council, Inc*; 2000.

17. EuroCode 8. Structure is seismic regions – Design. Part 1, General and Building. May 1988 Edition, *Report EUR 8849 EN*, Commission of European Communities

18. Vanmarke E.H. *SIMOKE: A Program for Artificial motion generation*. Civil Engineering Department, Massachusetts Institute of Technology; 1976.

19. Dwairi H.M. Equivalent damping in support of direct displacement-based design with applications to multi-span bridges. *Ph.D. Dissertation*; December 2004; North Carolina State University, Raleigh, North Carolina.

20. Chopra A.K. Dynamics of structures – theory and applications to earthquake engineering. *Prentice Hall*, New Jersey; second edition, 2001.